IEEE Access
Multidisciplinary | Rapid Review | Open Access Journal

Received March 22, 2021, accepted April 12, 2021, date of publication April 21, 2021, date of current version May 4, 2021.

Digital Object Identifier 10.1109/ACCESS.2021.3074581

A Multifunctional Non-Isolated Dual Input-Dual Output Converter for Electric Vehicle Applications

K. SURESH[1], C. BHARATIRAJA[1], (Senior Member, IEEE), N. CHELLAMMAL[1], (Member, IEEE), MOHD TARIQ[2], (Senior Member, IEEE), RIPON K. CHAKRABORTTY[3], (Member, IEEE), MICHAEL J. RYAN[3], (Senior Member, IEEE), AND BASEM ALAMRI[4], (Member, IEEE)

[1]Department of Electrical Engineering, SRM Institute of Science and Technology, Chennai 603203, India
[2]Department of Electrical Engineering, ZHCET, Aligarh Muslim University, Aligarh 202002, India
[3]Capability Systems Centre, School of Engineering and IT, UNSW Canberra at ADFA, Canberra, ACT 2612, Australia
[4]Department of Electrical Engineering, College of Engineering, Taif University, Taif 21944, Saudi Arabia

Corresponding authors: Mohd Tariq (tariq.ee@zhcet.ac.in) and C. Bharatiraja (bharatiraja@gmail.com)

This work was supported in part by the Taif University Researchers Supporting Project, Taif University, Taif, Saudi Arabia, under Grant TURSP-2020/278, and in part by the Project CRGS/Mohd Tariq/01 from the Hardware-In-the-Loop (HIL) Laboratory, Department of Electrical Engineering, Aligarh Muslim University, India.

ABSTRACT High voltage conversion dc/dc converters have perceived in various power electronics applications in recent times. In particular, the multi-port converter structures are the key solution in DC microgrid and electric vehicle applications. This paper focuses on a modified structure of non-isolated four-port (two input and two output ports) power electronic interfaces that can be utilized in electric vehicle (EV) applications. The main feature of this converter is its ability to accommodate energy resources with different voltage and current characteristics. The suggested topology can provide a buck and boost output simultaneously during its course of operation. The proposed four-port converter (FPC) is realized with reduced component count and simplified control strategy which makes the converter more reliable and cost-effective. Besides, this converter exhibits bidirectional power flow functionality making it suitable for charging the battery during regenerative braking of an electric vehicle. The steady-state and dynamic behavior of the converter are analyzed and a control scheme is presented to regulate the power flow between the diversified energy supplies. A small-signal model is extracted to design the proposed converter. The validity of the converter design and its performance behavior is verified using MATLAB simulation and experimental results under various operating states.

INDEX TERMS Multi-port converter, electric vehicle, bidirectional dc/dc converter, battery storage, regenerative charging.

I. INTRODUCTION

Increasing environmental pollution, the rapid rise in fuel cost, global warming, and depletion of fossil fuels have led to the development of advanced vehicle technologies. Therefore automobile industries have started manufacturing eco-friendly electric (EV) & hybrid electric vehicles (HEV). In such vehicles, the motor drive system is an important component. An efficient power electronic converter is required to propel the motor drive system. In the case of EV, this power electronic converter must possess the bidirectional capability to interface the energy resources with battery and motor drive systems. Numerous research work has been reported by the researchers in the literature on power electronic interfaces for EV systems. Different topologies of non-isolated three-port converter synthesized from dual input (DIC) or dual output (DOC) converter along with the single input single output (SISO) converter is dealt in [1]. A step-up converter combining the features of KY converter and buck-boost converter with a high voltage conversion ratio is presented in [2]. The method of improving the conversion efficiency using the interleaving concept in a double switch buck-boost converter is proposed [3]. A non-isolated boost converter with high voltage gain capable of balancing automatically under an unbalancing load condition is analyzed in [4]. Bang and Park [5] describe buck cascaded buck-boost power factor

The associate editor coordinating the review of this manuscript and approving it for publication was Xiaosong Hu.

TABLE 1. Components comparison.

Bidirectional Buck-Boost Converters in paper	No. of Inputs	No. of Outputs	No. of Inductors	No. of Switches	No. of Diodes	No. of Capacitors
H. Kang, et. al [4]	1	1	1	4	-	3
M. Badawy, et. al [7]	1	1	2	4	-	2
A. Hasanzadeh, et. al [8]	1	1	6	6	-	4
M. Reza Banaei, et. al [13]	1	1	2	1	2	3
A. Ajami, et. al [14]	1	1	3	1	2	4
B. Vural, et. al [18]	2	1	2	5	2	1
A. Khaligh, et. al [25]	1	1	1	5	5	2
T. K. Santhosh, et. al [26]	1	2	1	4	-	2
Proposed converter (FPC)	Single Input→Three Output (or) Double Input→Double Output		2	3	2	3

correction converter for wide input voltage variations. The above-mentioned converters are unidirectional with the SISO configuration. A non-isolated bidirectional dc/dc converter in [6] is a SISO model that uses four active switches. A comparison of two different bidirectional converters such as cascaded buck-boost capacitor in the middle and cascaded buck-boost inductor in the middle is carried out in [7]. To achieve high power density and enhance efficiency, zero-voltage transition three-level dc/dc converter with the soft switching feature is proposed [8]. The converter in [9] is a three-port bidirectional topology that uses three inductors and three active switches to produce either buck or boost output. Different structures of parallel buck-boost converters, converters with two modules of supercapacitors and their power management control strategies are well investigated in [10]. A Multi-port energy converter in [11] employs a single leg active switching element for the multi-functional operation to regulate and manage the output power. When comparing the above-said converter with the basic buck-boost converter, it uses more passive elements. A bidirectional high gain step-up/down dc converter in [12] which has been realized as a non-isolated structure has an in-built DC transformer which increases the size of the converter. The single-switch buck-boost topology presented in [13], [14] operates in SISO mode and it inherits the features of CUK converters and supersedes the problems encountered in KY converter. Non-isolated multi-input multi-output dc/dc converters presented in [15], [16] is a boost converter meant for photovoltaic applications with unidirectional power flow. The setback of a multi-input single-output n-stage converter in [17], [18] is that only (n-1) stages do the buck-boost operation and the nth stage operates as a boost converter with power transferred from source to load always. The circuit configuration in [19], [20] is designed with switched capacitor technique for multiple inputs applications. Here, the number of active and passive components used in this configuration equals the number of input sources, which in turn increases the circuit structure and control complexity. The utilization of single inductor based non-isolated multi-port converter proposed in [21], [22] is limited to low power applications one active switch for integrating diversified load devices. Multiport dc/dc converter in [23] is an isolated bidirectional converter. A Multi-winding transformer in it which helps in transferring the power increases the size of the converter. Different structures of multiport bidirectional dc/dc converters are derived with the combination of dc-link and magnetic coupling [24]. Fully directional universal dc/dc converter [25] operates as a SISO converter. A dual input dual output converter suitable for the hybrid electric vehicle is proposed [26]. It has the basic disadvantage of battery power not being boosted across the load. A solar power aided EV with battery backup has been in [27]. To catalyze the energy between the battery and solar in the above EV a dc/dc converter structure has been presented. The number of switches in this converter varies based on the number of battery modules (Say if there exists 'n' no. of battery modules, then the system requires '2n' numbers of switches for effective operation). For effective power management between the ultracapacitor and battery and to suppress the issues such as overcharging of ultracapacitor and high battery current during peak power, a fuzzy logic control based energy management strategy has been proposed [28].

The major contribution of this paper is to propose a single-stage transformerless four-port (FPC) bidirectional buck-boost converter with only three switches. Compared with the topologies presented in the literature (see Table 1), the proposed converter has advantages such as a modular structure with reduced component count and integration of diversified sources in the input with different voltage-current characteristics. Apart from the above-said features, the proposed converter can provide output less than the minimum input voltage (buck) or greater than the maximum input voltage (boost). The reduction of switching losses improves the efficiency of the proposed converter.

This paper is organized as follows. In Section II, the basic idea of developing FPC and its operation modes is presented. The dynamic model of the converter using small-signal analysis is given in Section III. Validation of functionalities of the proposed converter using experimental results and control strategy for power budgeting is illustrated in Section IV and V. Finally the conclusion is provided in Section VI.

II. PERFORMANCE ANALYSIS OF MULTIPORT BUCK-BOOST CONVERTER

A. STRUCTURE OF FPC TOPOLOGY

The use of a single energy resource cannot meet the load demand due to input power variations and dynamic load in the electric vehicular system. Therefore, the hybridization of arbitrary energy resources is required. This manuscript focuses on synthesizing a converter topology that could interface various energy resources with the drive train of a vehicle. Figure 1 (a) and (b) depict the role of power electronic interface in the power system of an electric vehicle system.

Figure 2 shows the proposed topology of a four-port (FPC) converter.

Prominent features of the proposed converter are:

- Bidirectional power flow capability
- Individual power flow control between the sources
- Easy design, control, and implementation process

As shown in Figure 2 the power flow between load and input sources is controlled by the controllable switches Q_1, Q_2, and Q_3. As seen from Figures 3a to 3e five different states of operation can be considered for the proposed converter. The state 1 is a (single input dual output) SIDO state. In this state (see Figure 3a), the drive train of EV (load) is powered by the power generated from PV. The battery in the proposed topology can be charged either from the input PV power or from the load (see Figure 3b & Figure 3e).

In state 5, due to regenerative braking the energy returning from the load is stored in the battery. Due to low irradiation and if the PV is not able to generate the power, the battery discharges to meet the entire load requirement (see Figure 3c). During peak power demand, the battery unit and PV provide the necessary power to drive train. The converter then operates in the DIDO state (see Figure 3d). Switching schemes of the proposed converter and equivalent circuits under different operating states are depicted in Figures 4 & 5 respectively.

B. OPERATING MODES- STATE OF OPERATION

1) STATE 1-SIDO (SINGLE INPUT DUAL OUTPUT) STATE OF THE CONVERTER (POWER TRANSFER FROM PV (Vdc) TO LOAD)

In this state, PV transfers the power individually to the load. The Switching schemes of various operating devices are shown in Table 2. Switches Q_1 and Q_3 are turned ON and,

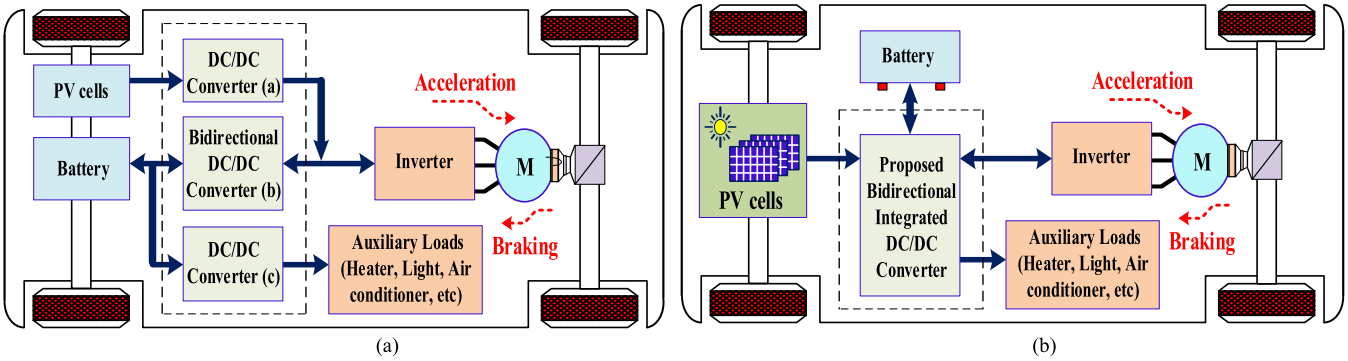

FIGURE 1. Block diagram of (a) Conventional converter (b) Proposed integrated four-port converter (FPC) interface in an electric vehicle system.

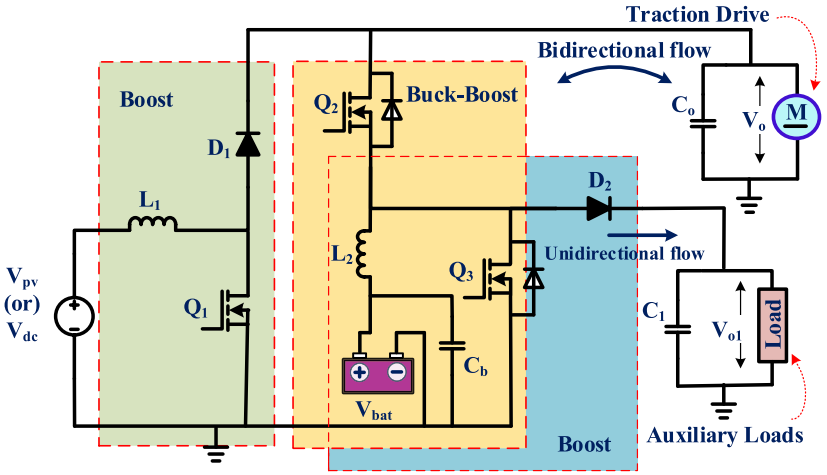

FIGURE 2. Topology diagram of four-port (FPC) converter.

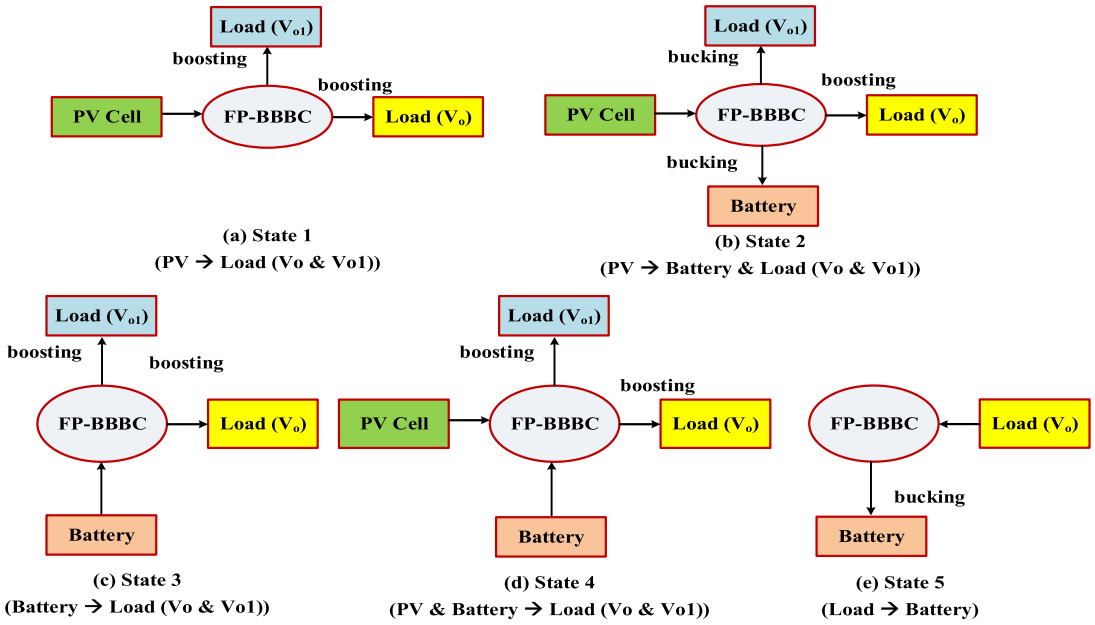

FIGURE 3. a) State 1(boost), b) State 2 (buck & boost), c) State 3 (boost), d) State 4 (boost), e) State 5 (buck).

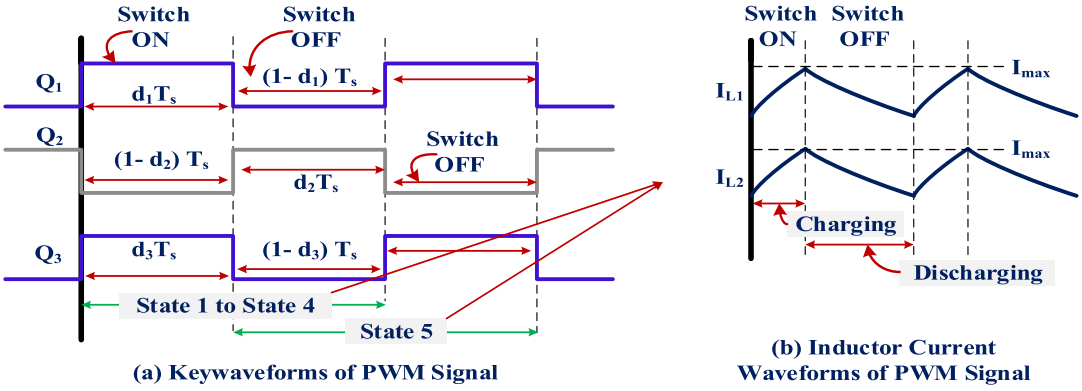

FIGURE 4. State of operation of proposed FPC.

Q_2 is turned OFF, during the time interval 0 to d_1T_s. While considering $V_{pv} > V_{bat}$ (see Figure 5 (a) and (b)), the voltage V_{pv} appears across the inductor L_1, resulting in the rise of inductor current with the positive slope. During time interval d_1T_s to T_s, switches Q_1, Q_3 are turned off and Q_2 is turned on. Energy stored in inductor L_1 during the previous time interval d_1T_s is discharged to the output capacitor through the diode D_1. Here T_s is the switching time period. Under steady- state operation, the output voltage is given by

$$V_o = \frac{1}{1\text{-}d_1} V_{pv} \tag{1}$$

$$V_{o1} = \frac{1}{1\text{-}d_1} V_{pv} \tag{2}$$

2) STATE 2- SITO (SINGLE INPUT THREE OUTPUT) STATE OF THE CONVERTER (POWER TRANSFER FROM PV TO BATTERY AND LOAD)

Operation in this state is similar to state 1. When the battery needs to be charged from PV (see Figure 5 (c) and (d)), Q_2 operates with $d_2 < 0.5$ to charge the battery. Q_3 operates similarly as that of Q_1 with $d_1 > 0.5$ to produce boosted output across the load. Voltages V_{bat}, V_{pv}, and V_o, V_{o1} are related by the equation

$$V_o = \frac{1}{1\text{-}d_1} V_{pv} \tag{3}$$

$$V_{o1} = d_2 V_{pv} \tag{4}$$

$$V_{bat} = d_2 V_{pv} \tag{5}$$

3) STATE 3 - SIDO STATE OF THE CONVERTER (POWER TRANSFER FROM THE BATTERY)

In this state, the energy stored in the battery is transferred to the load. During the time interval 0 to d_3T_s, discharging action of the battery causes the inductor current i_{L2} to rise linearly. Between the intervals d_3T_s to T_s, the current i_{L2} decreases with a negative slope. ON-OFF state of switch Q_3 provides a boosted output across the drive train. As Q_1 does not take part in transferring the energy from battery to

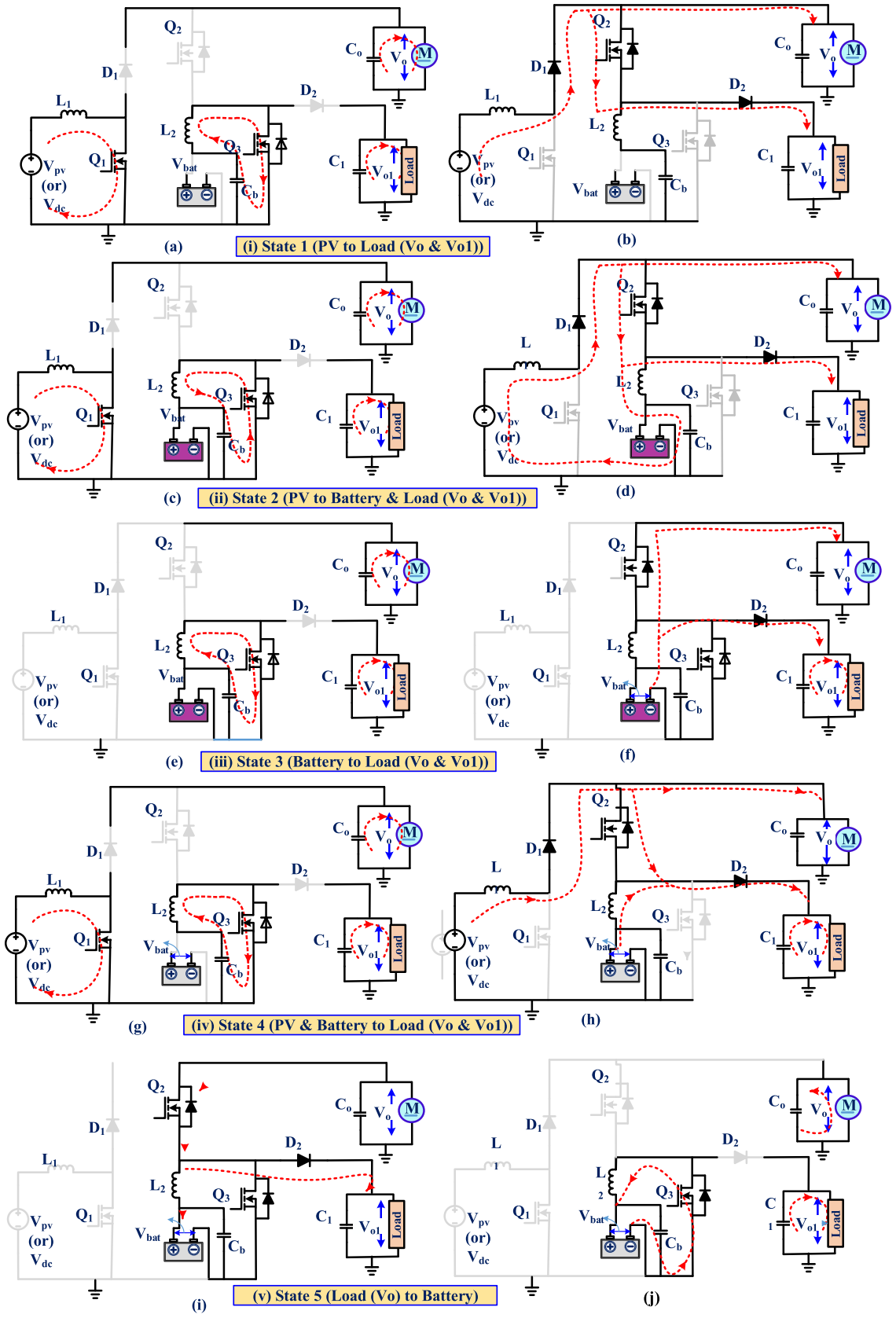

FIGURE 5. Typical diagram of all the states (i) State 1, (ii) State 2, (iii) State 3, (iv) State 4, & (v) State 5.

TABLE 2. State of operation.

No.of States	Input Sources	MOSFET Switches			Inductors		Diodes		Battery	Capacitors		Outputs	
		Q_1	Q_2	Q_3	L_1	L_2	D_1	D_2	V_{bat} (or) C_b	C_o	C_1	(V_o)	(V_{o1})
State 1 (V_{pv}>V_{bat})	(V_{pv}) or (V_{dc})	ON	OFF	ON	↑	↑	OFF	OFF	-	↓	↓	Boost	Boost
		OFF	ON	OFF	↓	↓	ON	ON		↑	↑		
State 2 (V_{pv}>V_{bat})	(V_{pv}) or (V_{dc})	ON	OFF	ON	↑	↓	OFF	OFF	↑	↓	↓	Boost	Boost
		OFF	ON	OFF	↓	↑	ON	ON		↑	↑		
State 3 (V_{pv}<V_{bat})	(V_{bat})	-	OFF	ON	-	↑	-	OFF	↓	↓	↓	Boost	Boost
		-	ON	OFF	-	↓	-	ON		↑	↑		
State 4 (V_{pv}=V_{bat})	(V_{pv}) and (V_{bat})	ON	OFF	ON	↑	↑	OFF	OFF	↓	↓	↓	Boost	Boost
		OFF	ON	OFF	↓	↓	ON	ON		↑	↑		
State 5 (V_{pv}=0, V_{bat}<V_{load})	Regenerative braking power	-	ON	OFF	-	↑	-	ON	↑	↓	↓	Buck	Buck
		-	OFF	ON	-	↓	-	OFF		↑	↑		

Table representation: **ON**- Switch close, **OFF**- Switch open, ↑- charging of inductor and capacitor, and ↓- discharge of inductor and capacitor

the load, it is kept in OFF condition throughout the state of operation (see Figure 5 (e) and (f)). The output voltage across the load due to discharging the battery is given as

$$V_o = \frac{1}{1\text{-}d_3} V_{bat} \tag{6}$$

$$V_{o1} = \frac{1}{1\text{-}d_3} V_{bat} \tag{7}$$

4) STATE 4 – DIDO (DUAL INPUT DUAL OUTPUT) STATE OF THE CONVERTER (POWER TRANSFER FROM PV AND BATTERY)

When the power demand from EV is high, the battery and PV supply, power to meet the demand (see Figure 5 (g) and (h)). During time interval 0 to $d_1 T_s$ gated switches Q_1 and Q_3 charge the inductor and cause the currents i_{L1} and i_{L2} to rise linearly. Q_2 is provided with the complimentary gate signal at this interval. On the other hand during the off period of switches Q_1, Q_3 the inductor currents i_{L1} and i_{L2} decrease with the negative slope. Thus boosted power from both battery and PV is delivered to the load via diodes D_1 and D_2. Net output voltage due to the power delivery of both the sources can be determined from Eqs.(8-9):

$$V_o = \frac{1}{1\text{-}d_1} V_{pv}, \text{ (or) } V_o = \frac{1}{1\text{-}d_3} V_{bat} \tag{8}$$

$$V_{o1} = \frac{1}{1\text{-}d_1} V_{pv}, \text{ (or) } V_{o1} = \frac{1}{1\text{-}d_3} V_{bat} \tag{9}$$

5) STATE 5 - SIDO STATE OF THE CONVERTER (POWER TRANSFER FROM LOAD TO BATTERY)

During regenerative braking, the kinetic energy stored in the drive train is fed back to the battery (see Figure 5 (i) and (j)). The switching sequence of this state is given as follows: Q_1 is permanently in the off condition; Q_2, Q_3 is turned ON and Q_2 is turned OFF. The ON-OFF state of Q_2 along with Q_3 charges the battery.

$$V_{bat} = d_2 V_o \tag{10}$$

In same state, the battery is suppled by the second output through regenerative braking power. The control relation is derived as,

$$V_{O1} = d_3 V_o \tag{11}$$

C. CONVERTER FAULT ANALYSIS

The converter fault condition is investigated as follows,

Case-1: If switch Q_1 opens, the boosted PV power will not be available as the diode D_1 will be reverse biased. The converter works in SIMO state and continues to power the loads with the available battery power. At, the same time the regenerative power if available will charge the battery with the aid of switches Q_2 and Q_3.

Case-2: If switch Q_2 opens, the PV module will not be able to power the auxiliary loads and the battery cannot be charged during regenerative braking. However, the PV modules will be able to drive the traction drive with its available power and the converter works in SISO state.

Case-3: If switch Q_3 opens, the charging and discharging action will be affected. Battery will not be able to deliver boosted output across the loads?

Case-4 Due to switching (ON-OFF) action, switch Q_1 delivers boosted output across the loads through diode D_1. But if diode D_1 opens, then the load will not be delivered with boosted output and there will be circulating current through the inductor L_1 and the switch which in turn will generate heat in the loop. Similarly, if the diode D_2 opens, there will not any power supplied through the diode D_2 to the load.

III. DYNAMIC MODELING

A proper control scheme is required to fix the duty cycles of an individual switch in the converter to regulate the output voltages, the charging, and discharging actions of the battery. Therefore, to design such controllers, dynamic modeling of the converter using a small-signal model needs to be obtained. The state-space average model of the four-port converter is derived based on the state-space description of the converter in each switching state. Following are the steps involved in deducing the average model

- Derivation of state-space equation during open /close condition of switches

- Averaging the deduced state equations
- Perturbation
- Matrix creation

To obtain the small-signal model, the current through the inductors and voltage across the capacitors are assumed as state variables. As five operating states of the presented converter use different combinations of the two input sources and produce either buck, boost, or buck-boost outputs simultaneously five different models can be obtained. State variables in equation (12), (13) and (14) consist of DC components (I, d, V) and perturbations ($\hat{i}$, $\hat{d}$, $\hat{v}$). Perturbations are assumed to have small variations over one switching period. Replacing the state parameters with the sum of steady- state parameters and perturbation values, the following constraints can be derived.

$$\begin{aligned} i_{L_1} &= I_{L_1} + \hat{i}_{L_1} \\ i_{L_2} &= I_{L_2} + \hat{i}_{L_2} \\ v_o &= V_o + \hat{v}_o \\ v_{o1} &= V_{o1} + \hat{v}_{o1} \end{aligned} \tag{12}$$

$$v_{bat} = V_{bat} + \hat{v}_{bat} \tag{13}$$

$$\begin{aligned} d_1 &= d_1 + \hat{d}_1 \\ d_2 &= d_2 + \hat{d}_2 \\ d_3 &= d_3 + \hat{d}_3 \end{aligned} \tag{14}$$

A. STATE 1 (V_{pv} → LOAD [BOOST OPERATION])

As the converter is considered to be operating in CCM, the switches (see Figure 5 (a) and (b)) Q_1 is ON, Q_2 is OFF for a period of d_1T_s, and Q_1 is OFF, Q_2 is ON for a period (1- d_1T_s). Substituting the perturbations, it is possible to obtain

$$\frac{d(\hat{v}_o)}{dt} = \left(\frac{1-d_1}{c_o}\right)\hat{i}_{L_1} - \left(\frac{\hat{d}_1}{c_o}\right)I_{l_1} - \left(\frac{1}{c_o r_o}\right)\hat{v}_o \tag{15}$$

$$\frac{d(\hat{v}_{o1})}{dt} = \left(\frac{1-d_1}{c_1}\right)\left(\hat{i}_{L_1} + \hat{i}_{L_2}\right) - \left(\frac{\hat{d}_1}{c_1}\right)\left(I_{l_1} + I_{l_2}\right) - \left(\frac{1}{c_1 r_1}\right)\hat{v}_{o1} \tag{16}$$

$$\hat{d}_1 I_{L_1} = (1-d_1)\,\hat{i}_{L_1} - \left(c_o + \frac{1}{r_o}\right)\hat{v}_o \tag{17}$$

$$\hat{d}_1 I_{L_1} = (1-d_1)\left(\hat{i}_{L_1} + \hat{i}_{L_2}\right) - \left(c_1 + \frac{1}{r_1}\right)\hat{v}_{o1} \tag{18}$$

From equation (15) to (18) we get,

$$\frac{1}{\hat{d}_1}\begin{bmatrix} \hat{i}_{L_1} \\ \hat{v}_o \\ \left(\hat{i}_{L_1} + \hat{i}_{L_2}\right) \\ \hat{v}_{o1} \end{bmatrix} = \begin{bmatrix} L_1 & (1-d_1) & 0 & 0 \\ (1-d_1) & \left(c_o + \frac{1}{r_o}\right) & 0 & 0 \\ 0 & 0 & (L_1+L_2) & (1-d_1) \\ 0 & 0 & (1-d_3) & \left(c_1 + \frac{1}{r_1}\right) \end{bmatrix}^{-1} \times \begin{bmatrix} I_{L_1} \\ V_o \\ (I_{L_1} + I_{L_2}) \\ V_{o1} \end{bmatrix} \tag{19}$$

B. STATE 2 (Vpv → Vbat & LOAD [BUCK & BOOST])

In this state, Q_1 and Q_3 are kept ON and Q_2 remains in the OFF state as in Figure 5 (c) and (d). Incorporating the perturbations are given as,

$$\frac{d_1(V_o + \hat{v}_o)}{dt} = \left(\frac{1-d_1-\hat{d}_1}{c_o}\right)(I_{L_1} + \hat{i}_{L_1}) - \left(\frac{1}{c_o r_o}\right)(V_o + \hat{v}_o) \tag{20}$$

$$\frac{d_2(V_{o1} + \hat{v}_{o1})}{dt} = \left(\frac{1}{c_o}\right)(I_{L_2} + \hat{i}_{L_2}) - \left(\frac{1}{c_1 r_1}\right)(V_{o1} + \hat{v}_{o1}) \tag{21}$$

$$\frac{d_2(V_{bat} + \hat{v}_{bat})}{dt} = \left(\frac{1}{c_b}\right)(I_{L_2} + \hat{i}_{L_2}) - \left(\frac{1}{c_b}\right)(V_{bat} + \hat{v}_{bat}) \tag{22}$$

$$\frac{1}{\hat{d}_1 \& \hat{d}_2 \& \hat{d}_3}\begin{bmatrix} \hat{i}_{L_1} \\ \hat{i}_{L_2} \\ \hat{v}_o \\ \hat{v}_{bat} \\ \hat{v}_{o1} \end{bmatrix} = \begin{bmatrix} L_1 & 0 & (1-d_1) & 0 \\ 0 & 0 & 0 & (-d_2) \\ (1-d_1) & 0 & -\left(c_o + \frac{1}{r_o}\right) & 0 \\ 0 & -1 & 0 & -1 \\ (1-d_3) & 0 & -\left(c_1 + \frac{1}{r_1}\right) & 0 \end{bmatrix}^{-1} \begin{bmatrix} V_o \\ V_{bat} \\ V_{o1} \\ I_{L_1} \\ I_{L_2} \end{bmatrix} \tag{23}$$

C. STATE 3 (Vbat → LOAD [BOOST])

During this state, the switch Q_3 is ON and Q_2 is OFF condition, inductor L_2 is charged. Switch Q_3 is OFF and Q_2 is ON, inductor L_2 is discharged from Figure 5 (e) and (f). Small-signal equations that can be deduced are

$$\frac{1}{\hat{d}_3}\begin{bmatrix} \hat{i}_{L_2} \\ \hat{v}_{o1} \\ \hat{v}_o \end{bmatrix} = \begin{bmatrix} L_2 & (1-d_3) & 0 \\ (1-d_3) & \left(c_1 + \frac{1}{r_1}\right) & 0 \\ 0 & (1-d_3) & \left(c_o + \frac{1}{r_o}\right) \end{bmatrix}^{-1} \times \begin{bmatrix} I_{L_2} \\ V_{o1} \\ V_o \end{bmatrix} \tag{24}$$

D. STATE 4 (Vpv and Vbat → LOAD [BOOST])

As state 4 combines the operation (see Figure 5 (g) and (h)) of state 1 and state 3, the average model of the converter with

the switching sequence shown in Table 2 can be derived as

$$\frac{1}{\hat{d}_1 \& \hat{d}_3}\begin{bmatrix}\hat{i}_{L_1}\\ \hat{v}_o\\ \hat{i}_{L_2}\\ \hat{v}_{o1}\end{bmatrix} = \begin{bmatrix} L_1 & (1-d_1) & 0 & 0\\ (1-d_1) & \left(c_o+\frac{1}{r_o}\right) & 0 & 0\\ 0 & 0 & L_2 & (1-d_3)\\ 0 & 0 & (1-d_3) & \left(c_1+\frac{1}{r_1}\right)\end{bmatrix}^{-1} \times \begin{bmatrix} I_{L_1}\\ V_o\\ I_{L_2}\\ V_{o1}\end{bmatrix} \quad (25)$$

E. STATE 5 (LOAD → Vbat [BUCK AND BOOST])

This state can be called as a regenerating state as the load power is negative. To store the regenerative braking energy in the battery, Q_1 is kept OFF, Q_2, and Q_3 are controlled as shown in Figure 5 (i) and (j). During regenerative operation, since the output voltage is greater than V_{pv}, the converter operates in buck mode and charges the battery. Averaging the state equations over one period, the small-signal model can be deduced as in equation below:

$$\frac{d(I_{L_2}+\hat{i}_{L_2})}{dt} = \left(\frac{d_2-\hat{d}_2}{L_2}\right)v_{brake} - \left(\frac{1}{L_2}\right)(v_{bat}+\hat{v}_{bat}) \quad (26)$$

$$\frac{d(V_o+\hat{v}_o)}{dt} = \left(\frac{I_{L_2}+\hat{i}_{L_2}}{c_b}\right) - \left(\frac{v_{bat}+\hat{v}_{bat}}{c_b}\right) \quad (27)$$

$$\frac{d(\hat{i}_{L_2})}{dt} = -\frac{v_{bat}}{L_2} - \frac{\hat{v}_{bat}}{L_2} \quad (28)$$

$$\frac{d(\hat{v}_{bat})}{dt} = \left(\frac{I_{L_2}+\hat{i}_{L_2}}{c_b}\right) - \left(\frac{\hat{v}_{bat}}{c_b}\right) \quad (29)$$

$$\frac{1}{\hat{d}_2}\begin{bmatrix}\hat{i}_{L_2}\\ \hat{v}_{bat}\end{bmatrix} = \begin{bmatrix}-L_2 & -1\\ -1 & (1+c_b)\end{bmatrix}^{-1}\begin{bmatrix}I_{L_2}\\ V_{bat}\end{bmatrix} \quad (30)$$

In summary, the five operating states are discussed and the small-signal model of the transfer function $\left(\frac{\text{Output voltage}}{\text{Duty cycle}}\right)$ is used for the closed-loop analysis of the proposed FPC converter.

IV. CONTROL STRATEGY AND HARDWARE RESULTS

The primary source is considered to be a photovoltaic (PV) panel of 100 W (two Mono crystalline 50W PV panel) and a 12 V, 7Ah battery is considered to be a storage element. The PV panel is connected with conventional P&O MMPT controller to find out the maximum power point (MPP). To demonstrate various operating modes with different combinations of input/output voltages, a small scale prototype model of the proposed converter with a lower rating is built as shown in Figure 7. Details of the experimental setup are provided in Table 3. The controlled switches in the power circuit are realized using MOSFET (IRFP250N) and the uncontrolled switches with diodes UF5408. Switch and state selection control algorithms shown in Figure 6 are embedded in the PIC controller (dsPIC30F2010). The simple PI controller is used to generate the duty cycles of the MOSFETs Q_1, Q_2 and Q_3 as shown in Fig.6 (b). The duty cycles of Q_1, Q_2 and Q_3 are given in Fig.6(c). The reference output voltages (V_{o_ref} and V_{01_ref}) and actual load output voltages (V_o and V_{01}) are compared and error is generated to find out the current references (I_{L1ref} and I_{L2ref}). The k_p and k_i values of the PI controller is found from MATLAB auto turning and imported to dsPIC30F2010 controller. The current

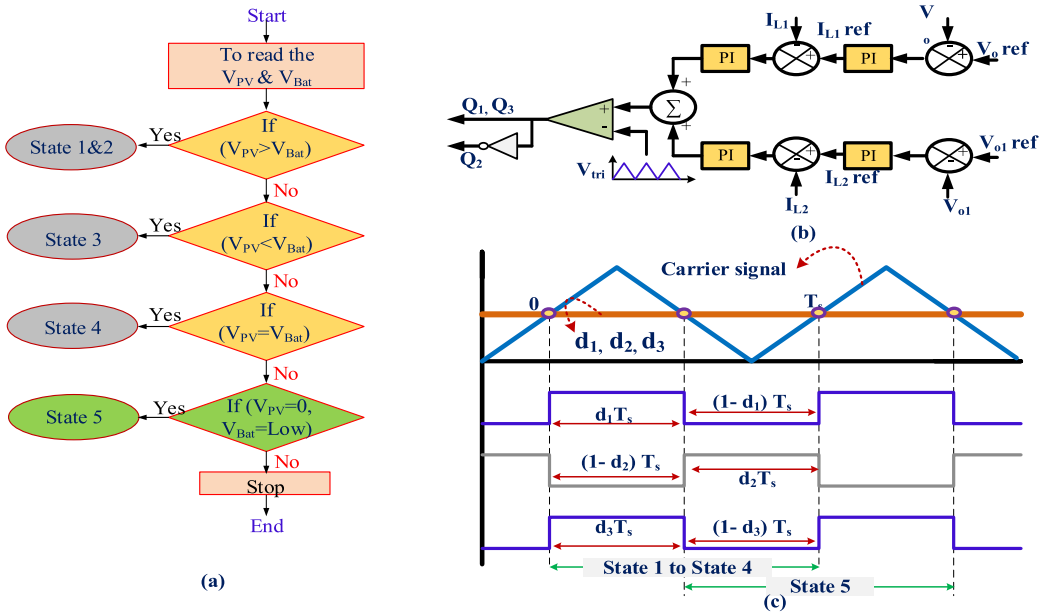

FIGURE 6. Proposed FPC (a) Flow chart (b) PWM generator with PI control (c) duty cycle.

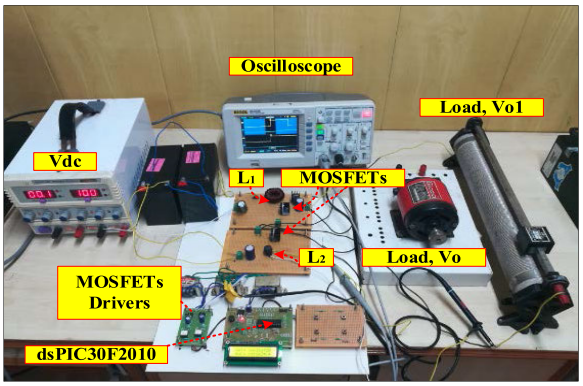

FIGURE 7. Experimental setup of the proposed converter.

TABLE 3. Setup configuration.

Components	Ratings
Capacitor (C_1 & C_o)	1000μF, 63V
Diode (D_1 & D_2)	UF5408(V_F =1.7V,3A,50 to 1000 V)
MOSFET	IRFP250N (V_{DS} =0.27V, 30A,200V, 0.075Ω)
Inductor (L_1)	1mH
Inductor (L_2)	120μH
Battery	12V, 7Ah, (*Lead-Acid*)

error determines the reference signals of Q_1, Q_2 duty cycle. The 10 kHz triangle carrier signal and reference signal are compared to generate the duty cycles of Q_1, Q_2. The switches Q1 and Q3 are operated simultaneously with same duty cycles and Q2 in complimentary fashion. Hence the NOT gate is used to generate the Q2 duty cycles.

A. STATE 1 & 2

Microcontroller process the feedback signals and provide the controlled duty cycles required for the converter to operate in a particular state (see Figure 8(i) and 8(ii)). For an example, the controller reads V_{pv}& V_{bat} and selects state 1 & 2 if $V_{pv} > V_{bat}$. After the state selection, based on the PWM switching algorithm, switches Q_1 is triggered and the converter works in SIDO state. A boosted output V_o & $V_{o1} = 69$ V (see Figure 8 (i)) & $I_{out} = 1.37$ A are available across the load for the given $V_{pv} = 21$ V & $I_{pv} = 4.6$ A.

B. STATE 3

If $V_{pv} < V_{bat}$, then state 3 is selected and the converter will operate similarly to state 1 with battery as rimary source. Now the battery (where $V_{bat} = 12$ V, $I_{bat} = 8.02$ A) which has charged in the previous cycle discharges to provide boosted output of V_o & $V_{o1} = 58$ V &, $I_{out} = 1.63$ A as shown in Figure 8(iii).

C. STATE 4

If $V_{pv} = V_{bat}$, then the converter works in state 4 (DIDO). Here the primary source (V_{pv}) along with battery supplies power to the load to meet the expected demand. The experimental results for this state of operation are presented in Figure 8(iv). From Figure 8(iv), it is seen that when $V_{pv} = 20$ V, $I_{pv} = 4.81$ A, $V_{bat} = 20$ V, $I_{bat} = 4.81$ A, V_o & $V_{o1} = 38$ V, $I_o = 2.49$ A.

D. STATE 5

State change is effected when load power is greater than the input power (during regenerative braking). The motor drive in EV delivers power in the reverse direction. The brake power is recovered and the battery is charged due to the bucking operation of the converter. Figure 8(v) illustrates that when $V_{o\,(brake)} = 34$ V & $I_{o\,(brake)} = 2.81$ A, the charging voltage and current are about $V_{bat} = 10.2$ V & $I_{bat} = 9.3$ A.

Considering the electric vehicle application, the converter should have a more control degree of freedom. With this aim, the converter is involved with different load duty cycles operation and the results are tabulated in table 4. Based on the results, it can be seen that the proposed converter has more degree of freedom with its control and able to provide a wider output voltage.

TABLE 4. Experimental results.

No.of States	Input Voltage		MOSFET Duty Cycle			Output Voltages		Output Status
	(V_{dc})	(V_{Bat})	Q_1	Q_2	Q_3	(V_o)	(V_{o1})	(V_o)& (V_{o1})
State 1 ($V_{pv}>V_{bat}$)	21	Not in use	69%	50%	50%	69	69	Boost
	22	18	50%	50%	50%	42.81	41.47	Boost
State 2 ($V_{pv}>V_{bat}$)	21	7.1	68%	32%	68%	66	66	Boost
	22	15	50%	50%	50%	41.92	39.69	Boost
State 3 ($V_{pv}<V_{bat}$)	Not in use	12	50%	21%	79%	58	58	Boost
	Not in use	22	50%	50%	50%	46.15	45.38	Boost
	18	22	50%	50%	50%	46.15	45.38	Boost
State 4 ($V_{pv}=V_{bat}$)	20	20	47%	53%	47%	38	38	Boost
	25	25	50%	50%	50%	52.37	51.57	Boost
State 5 ($V_{pv}=0$, $V_{bat}<V_{load}$)	Not in use	10.2	30%	70%	30%	34	34	Buck
	Not in use	10.95	50%	50%	50%	22	21.36	Buck
	Not in use	12.88	70%	30%	70%	52	50.99	Buck

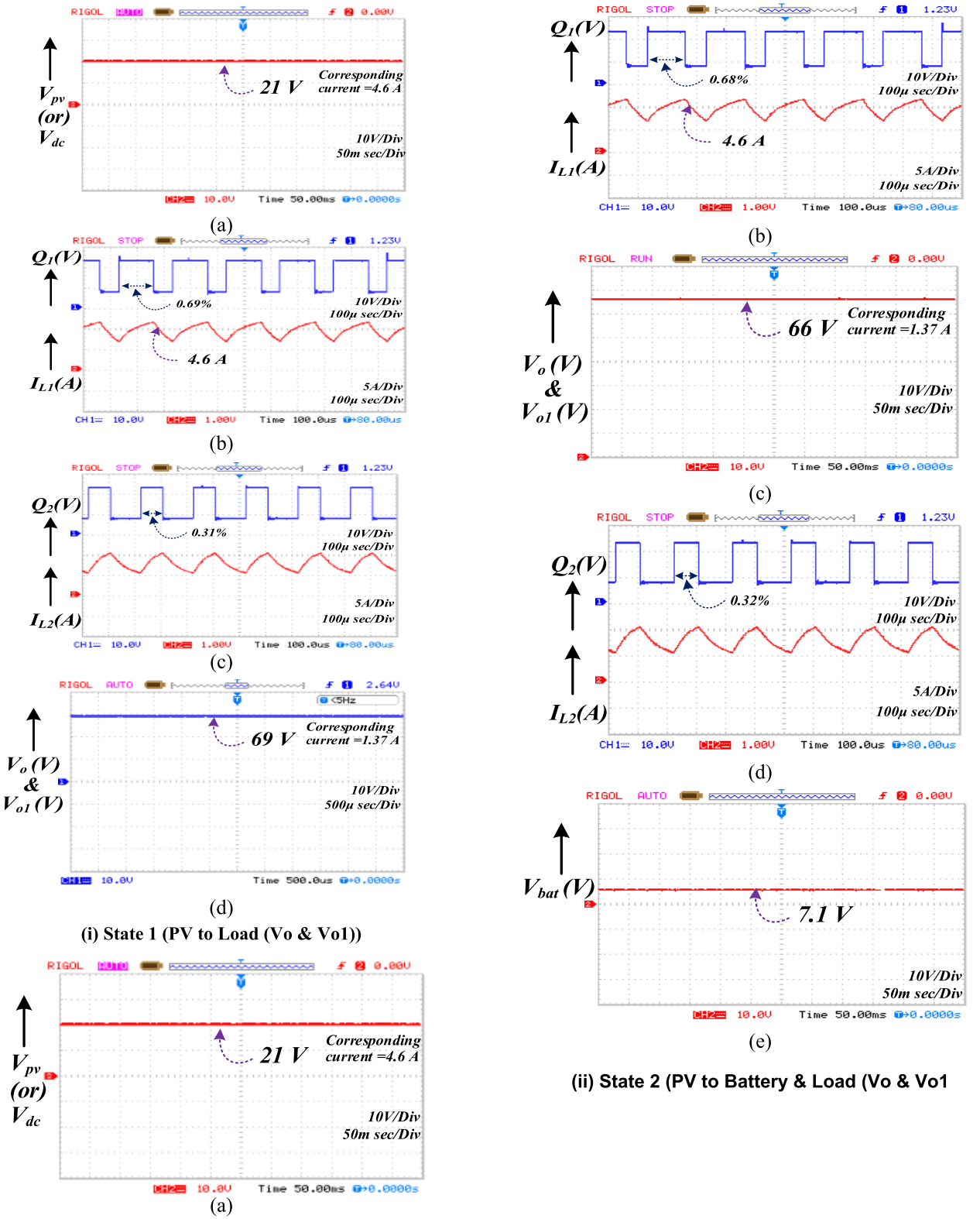

(i) State 1 (PV to Load (Vo & Vo1))

(ii) State 2 (PV to Battery & Load (Vo & Vo1

FIGURE 8. Experimental results of all the states: (i) State 1, (ii) State 2, (iii) State 3, (iv) State 4, & (v) State 5.

With the help of state space model obtained in various operating states, the dynamic behaviour of the proposed four port converter against sudden variations in input voltage and load is analysed and depicted in Figure 8.

For an example, in State 1 (Figure 9(i)) the input voltage is decreased from 22V to 20 V and suddenly increased to a value of 25 V higher than the given input voltage. The step down and step up voltage are regulated by the duty ratios d1 and

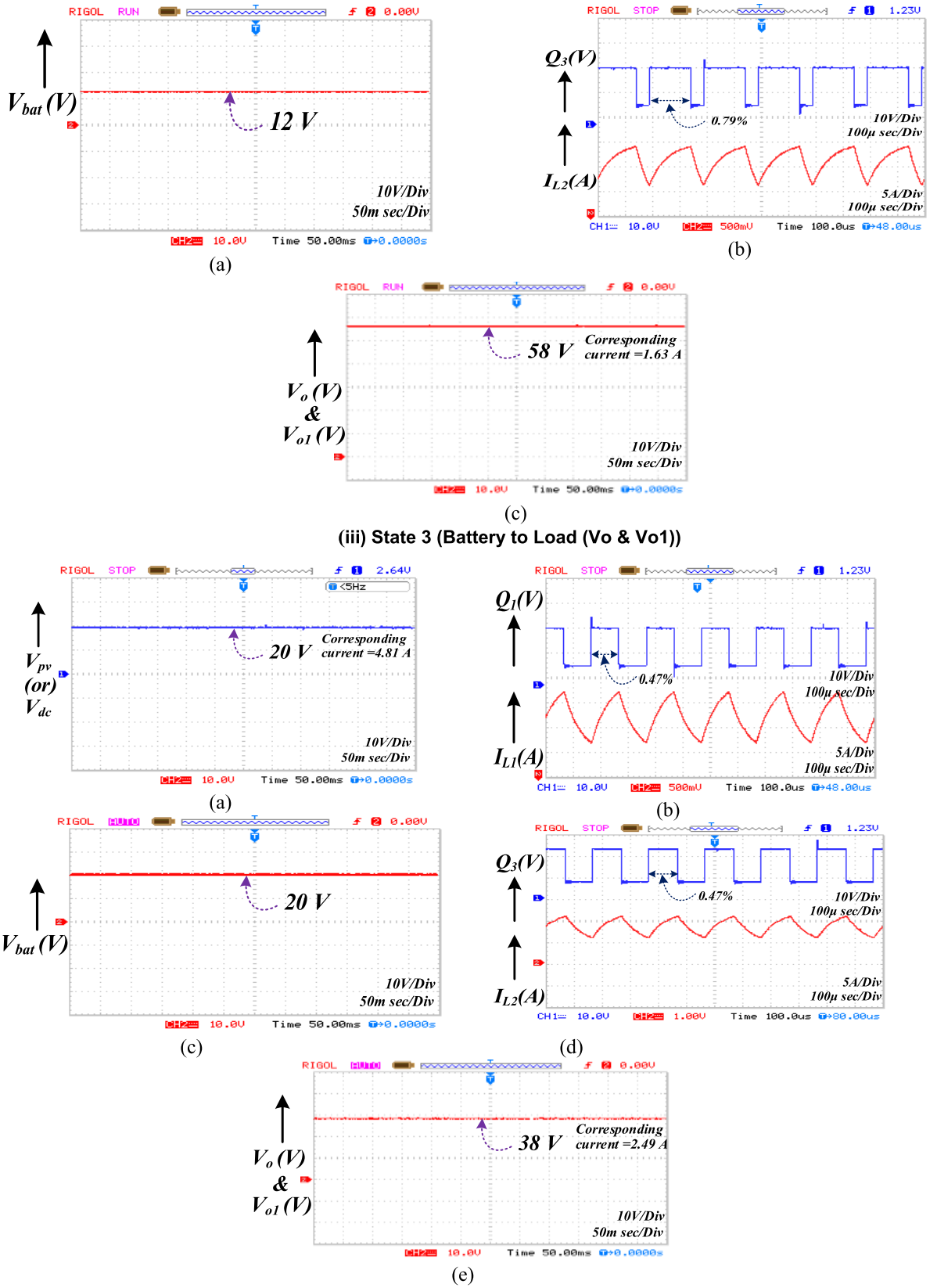

FIGURE 8. *(Continued.)* **Experimental results of all the states: (i) State 1, (ii) State 2, (iii) State 3, (iv) State 4, & (v) State 5.**

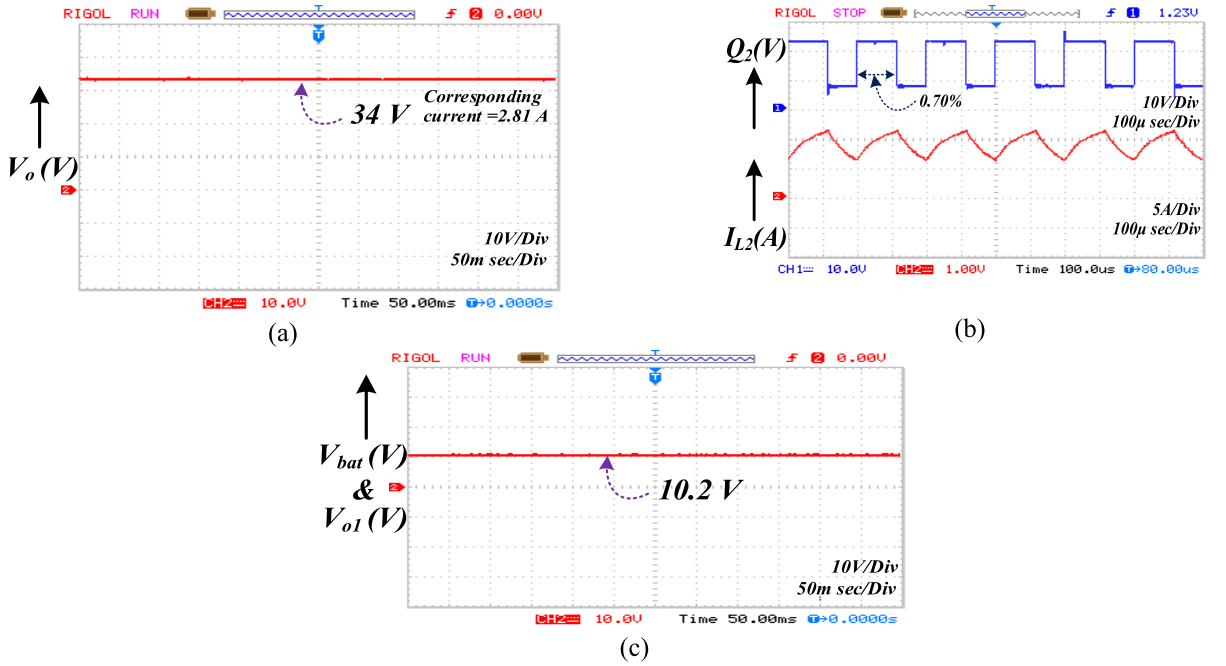

FIGURE 8. *(Continued.)* **Experimental results of all the states: (i) State 1, (ii) State 2, (iii) State 3, (iv) State 4, & (v) State 5.**

d2. Applying the concept of line regulation, the ability of the controller to compensate for approximately 9% decrease in input voltage and 14% increase in input voltage is well depicted in Figure 9.i and 9 ii. The load regulation ability of the controller against 20% step increase and step decrease in R01 is shown in Figure 9.iii and 9 d. This shows the designed controller is able to fix the output voltages of 42.81 V and 42.67 V across the two loads irrespective of any load or input changes. Output load voltages changes is given in the Figure 9.iv.

Battery SoC and SoH Measurement: During state-3 and state-4, Battery discharges to supply power to the load and during state 5, the load supplies the power to battery (battery is charging). The experiment is performed with the initial battery SoC of 45.1256%. During the time of state-3 and state-4, the Battery SoC is reduced gradually (battery discharges). The measured SoC at the end of state-4 is observed as 45.0345 %. The change in SoC is very minimal as the states operation time is very small as the states are exercised in high switching frequency interval. Similarly during state-5 the battery SoC is increased to from 45.0345 to 45.0526%. The SoH values are also calculated from state-1 beginning to end of state-5 as 80.001 to 8.002.

V. EFFICIENCY-LOSS ANALYSIS

Having conventional buck, boost, and buck-boost converter as reference; switching losses of the proposed converter can be estimated for different operating conditions. Since the proposed converter operates like a conventional boost converter in state 3, state 4, and buck converter in state 5, it does not encounter any additional losses. Therefore, the comparative change-inefficiency need to be calculated individually for state 1 and state 2 only. In state 1 when the converter operates like a conventional boost converter, the additional conduction loss which is due to Q2 can be written as,

$$\Delta p_{LOSS_1} = p_{Q_2} \text{ (boost)} \tag{31}$$

Similarly, state 2 the converter operates in buck mode, it charges the battery from source1 (PV), and during boost mode it interconnects the load and PV. Therefore, a change in loss can be calculated as

$$\Delta p_{LOSS_2} = p_{Q2} \text{ (boost)} \tag{32}$$

$$\Delta p_{LOSS_2} = p_{D_1} + p_{Q_1} \text{ (buck)} \tag{33}$$

Thus, the efficiency can be calculated as,

$$\Delta\eta = \eta - \eta' = \frac{P_O}{P_{IN}} - \frac{P_O}{P_{IN} + \Delta P_{LOSS}} \tag{34}$$

here $\Delta\eta$ is the change in efficiency, η is the efficiency of the conventional buck-boost converter and η' is the efficiency of the proposed buck-boost converter. P_{IN} and P_O are the input and output power. Fig.10 shows the efficiency calculation of state 1 to sate 4.

- *State 1*

During boost mode

$$\Delta\eta_1 = \eta_1 - \eta_1' = \frac{69 \times 1.37}{21 \times 4.6} - \frac{69 \times 1.37}{(21 \times 4.6) + [(0.27 \times 1.37)]}$$

$$\Delta\eta_1 = \frac{94.53}{96.6} - \frac{94.53}{96.6 + 0.3699}$$

$$\Delta\eta_1 = 0.9785 - 0.9748 = 0.37\%$$

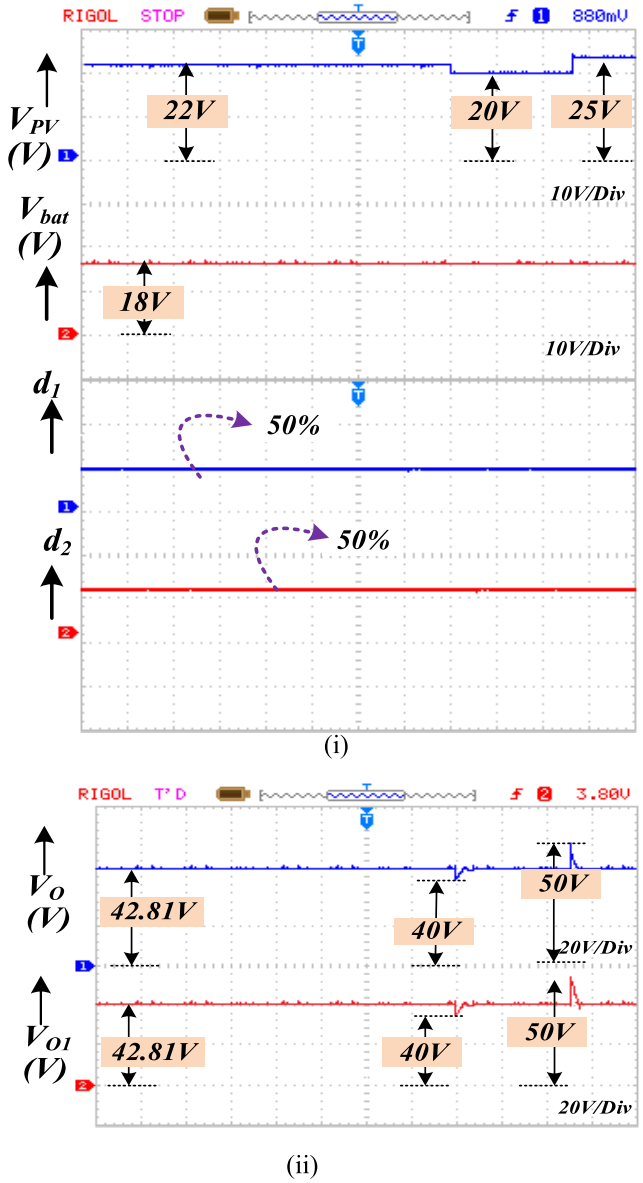

FIGURE 9. Experimental results with change in input voltage change in duty cycle and load: (i) Change in PV voltage, constant battery voltage, and constant duty cycle, (ii) Vo and Vo1, (iii) Change constant duty cycle, when constant PV voltage and battery voltage, (iv) Output load voltages.

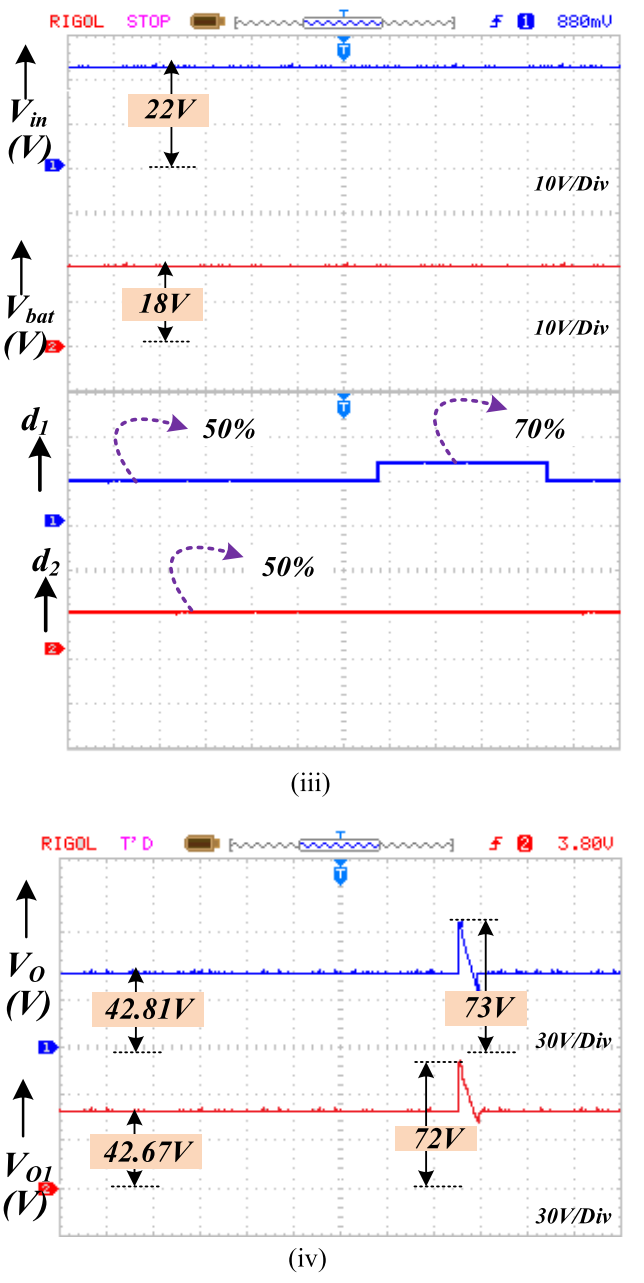

FIGURE 9. *(Continued.)* Experimental results with change in input voltage change in duty cycle and load: (i) Change in PV voltage, constant battery voltage, and constant duty cycle, (ii) Vo and Vo1, (iii) Change constant duty cycle, when constant PV voltage and battery voltage, (iv) Output load voltages.

- *State 2*

During boost mode

$$\Delta\eta_1 = \eta_1 - \eta_1' = \frac{69 \times 1.37}{21 \times 4.6} - \frac{69 \times 1.37}{(21 \times 4.6) + [(0.27 \times 1.37)]}$$

$$\Delta\eta_1 = \frac{94.53}{96.6} - \frac{94.53}{96.6 + 0.3699}$$

$$\Delta\eta_1 = 0.9785 - 0.9748 = 0.37\%$$

During buck mode

$$\Delta\eta_2 = \eta_2 - \eta_2' = \frac{7.1 \times 13.5}{21 \times 4.6} - \frac{7.1 \times 13.35}{(21 \times 4.6) + [(1.7 \times 13.5) + (0.27 \times 4.6)]}$$

$$\Delta\eta_2 = \frac{95.85}{96.6} - \frac{95.85}{96.6 + 22.95 + 1.242}$$

$$\Delta\eta_2 = 0.9922 - 0.7935 = 19.87\%$$

Loss beardown

The converter overall efficiency ranges between 97.6% to 98.4%. The loss breakdown for the proposed converter is shown in the Fig.11. The total loss of the converter is observed in the range of 3.4W to 1.6W. Here the switching and conduction losses of the MOSFET are observed as 8% and 11% respectively. The diode conduction losses are observed as 5%.

TABLE 5. Components comparison.

Bidirectional Buck-Boost Converters in paper	No. of Inputs	No. of Outputs	No. of Passive Element used	No. of used Switches/Diode	Converter Efficiency
H. Kang, et. al [4]	1	1	4	4/ Not use	98.2%
M. Badawy, et. al [7]	1	1	4	4/ Not use	96.6%
A. Hasanzadeh, et. al [8]	1	1	10	6/ Not use	97.8%
M. Reza Banaei, et. al [13]	1	1	5	1/2	92.6%
A. Ajami, et. al [14]	1	1	7	1/2	93.2%
B. Vural, et. al [18]	2	1	3	5/2	98.6%
A. Khaligh, et. al [25]	1	1	3	5/5	97.2%
T. K. Santhosh, et. al [26]	1	2	3	4/ Not use	92.6%
Proposed converter (FPC)	Single Input→Three Output (or) Double Input→Double		2	3/2	98.2%

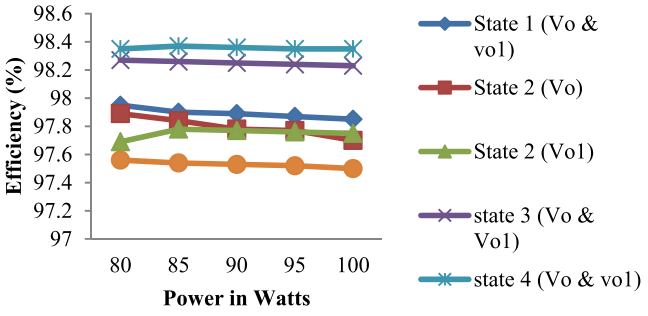

FIGURE 10. Efficiency waveforms with different Power in Watts.

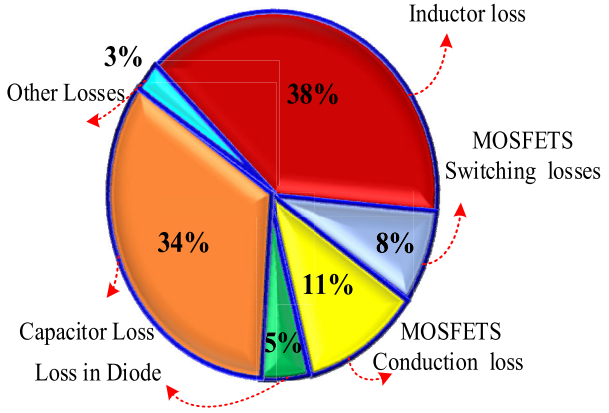

FIGURE 11. Loss breakdown for the proposed converter.

Expect this MOSFET and Diode losses, the converter other losses in their passive components losses is around 75%.

The proposed converter efficiency calculation is extended for California Energy Commission (CEC) efficiency and European efficiency. The CEC efficiency is a weighted average of measurements taken at different power levels and input voltages. The European efficiency is a weighted average at a single input voltage. The observed CEC efficiency of 98.2% while European efficiency is 97.6%.

The Table 1 shows the proposed topology efficiency, passive elements and switches used is compared with different similar converter topology. From the results it can see that the proposed converter efficiency is competing with other converters. In addition the proposed converter has advantages such as a modular structure with reduced component count and integration of diversified sources in the input with different voltage-current characteristics. This type converter can be used for HEV power circuit. In particularly the proposed converter can be used in regenerative operation.

VI. CONCLUSION

A single-stage four-port (FPC) buck-boost converter for hybridizing diversified energy resources for EV has been proposed in this paper. Compared to the existing buck-boost converter topologies in the literature, this converter has the advantages of a) producing buck, boost, buck-boost output even without the use of an additional transformer b) having bidirectional power flow capability with reduced component count c) handling multiple resources of different voltage and current capacity. Mathematical analysis has been carried out to illustrate the functionalities of the proposed converter. A simple control algorithm has been adopted to budget the power flow between the input sources. Finally, the operation of this converter has been verified through a low voltage prototype model. Experimental results validate the feasibility of the proposed four-port buck-boost topology.

ACKNOWLEDGEMENT

The authors would like to acknowledge the financial support from Taif University Researchers Supporting Project Number (TURSP-2020/278), Taif University, Taif, Saudi Arabia. The authors also acknowledge the financial support provided by the collaborative research grant scheme [CRGS/MOHD TARIQ/01] project, from the Hardware-In-the-Loop (HIL) Laboratory, Department of Electrical Engineering, Aligarh Muslim University, India.

REFERENCES

[1] H. Wu, Y. Xing, Y. Xia, and K. Sun, "A family of non-isolated three-port converters for stand-alone renewable power system," *IEEE Trans. Power Electron.*, vol. 1, no. 11, pp. 1030–1035, 2011.

[2] K. I. Hwu, K. W. Huang, and W. C. Tu, "Step-up converter combining KY and buck-boost converters," *Electron. Lett.*, vol. 47, no. 12, pp. 722–724, Jun. 2011.

[3] H. Xiao and S. Xie, "Interleaving double-switch buck–boost converter," *IET Power Electron.*, vol. 5, no. 6, pp. 899–908, Jul. 2012.

[4] H. Kang and H. Cha, "A new nonisolated High-Voltage-Gain boost converter with inherent output voltage balancing," *IEEE Trans. Ind. Electron.*, vol. 65, no. 3, pp. 2189–2198, Mar. 2018.

[5] T. Bang and J.-W. Park, "Development of a ZVT-PWM buck cascaded buck–boost PFC converter of 2 kW with the widest range of input voltage," *IEEE Trans. Ind. Electron.*, vol. 65, no. 3, pp. 2090–2099, Mar. 2018.

[6] C.-C. Lin, L.-S. Yang, and G. W. Wu, "Study of a non-isolated bidirectional DC–DC converter," *IET Power Electron.*, vol. 6, no. 1, pp. 30–37, Jan. 2013.

[7] M. A. Khan, A. Ahmed, I. Husain, Y. Sozer, and M. Badawy, "Performance analysis of bidirectional DC–DC converters for electric vehicles," *IEEE Trans. Ind. Appl.*, vol. 51, no. 4, pp. 3442–3452, Jul. 2015.

[8] S. Dusmez, A. Khaligh, and A. Hasanzadeh, "A zero-voltage-transition bidirectional DC/DC converter," *IEEE Trans. Ind. Electron.*, vol. 62, no. 5, pp. 3152–3162, May 2015.

[9] H. Zhu, D. Zhang, B. Zhang, and Z. Zhou, "A nonisolated three-port DC–DC converter and three-domain control method for PV-battery power systems," *IEEE Trans. Ind. Electron.*, vol. 62, no. 8, pp. 4937–4947, Aug. 2015.

[10] M. B. Camara, H. Gualous, F. Gustin, and A. Berthon, "Design and new control of DC/DC converters to share energy between supercapacitors and batteries in hybrid vehicles," *IEEE Trans. Veh. Technol.*, vol. 57, no. 5, pp. 2721–2735, Sep. 2008.

[11] T. Kim and S. Kwak, "Single pole switch leg based multi-port converter with an energy storage," *IET Power Electron.*, vol. 9, no. 6, pp. 1322–1330, May 2016.

[12] H. Wu, Y. Lu, L. Chen, P. Xu, X. Xiao, and Y. Xing, "High step-up/step-down non-isolated BDC with built-in DC-transformer for energy storage systems," *IET Power Electron.*, vol. 9, no. 13, pp. 2571–2579, Oct. 2016.

[13] A. Ajami, H. Ardi, and A. Farakhor, "Design, analysis and implementation of a buck-boost DC–DC converter," *IET Power Electron.*, vol. 7, no. 7, pp. 1906–1914, Nov. 2014.

[14] M. R. Banaei, H. Ardi, and A. Farakhor, "Analysis and implementation of a new single switch buck-boost DC–DC converter," *IET Power Electron.*, vol. 7, no. 12, pp. 2902–2913, May 2014.

[15] E. Babaei and O. Abbasi, "Structure for multi-input multi-output DC–DC boost converter," *IET Power Electron.*, vol. 9, no. 1, pp. 9–19, Jan. 2016.

[16] A. Nahavandi, M. T. Hagh, M. B. B. Sharifian, and S. Danyali, "A non-isolated multiinput multioutput DC–DC boost converter for electric vehicle applications," *IEEE Trans. Power Electron.*, vol. 30, no. 4, pp. 1818–1835, Apr. 2015.

[17] M. R. Banaei, H. Ardi, R. Alizadeh, and A. Farakhor, "Non-isolated multi-input–single-output DC/DC converter for photovoltaic power generation systems," *IET Power Electron.*, vol. 7, no. 11, pp. 2806–2816, Nov. 2014.

[18] F. Akar, Y. Tavlasoglu, E. Ugur, B. Vural, and I. Aksoy, "A bidirectional nonisolated multi-input DC–DC converter for hybrid energy storage systems in electric vehicles," *IEEE Trans. Veh. Technol.*, vol. 65, no. 10, pp. 7944–7955, Oct. 2016.

[19] Y. Yuan-Mao and K. W. E. Cheng, "Multi-input voltage-summation converter based on switched-capacitor," *IET Power Electron.*, vol. 6, no. 9, pp. 1909–1916, Nov. 2013.

[20] Y. Ye and K. W. E. Cheng, "Multi-port voltage-subtracting circuit based on resonant switched-capacitor," *IET Power Electron.*, vol. 5, no. 6, pp. 693–701, Jul. 2012.

[21] Y. Ye and K. W. E. Cheng, "Single-switch single-inductor multi-output pulse width modulation converters based on optimised switched-capacitor," *IET Power Electron.*, vol. 8, no. 11, pp. 2168–2175, Nov. 2015.

[22] H. Behjati and A. Davoudi, "Single-stage multi-port DC–DC converter topology," *IET Power Electron.*, vol. 6, no. 2, pp. 392–403, Feb. 2013.

[23] D. Gunasekaran and L. Umanand, "Integrated magnetics based multi-port bidirectional DC–DC converter topology for discontinuous-mode operation," *IET Power Electron.*, vol. 5, no. 7, pp. 935–944, Aug. 2012.

[24] H. Tao, A. Kotsopoulos, J. L. Duarte, and M. A. M. Hendrix, "Family of multiport bidirectional DC–DC converters," *IEE Proc.-Electr. Power Appl.*, vol. 153, no. 3, pp. 451–458, May 2006.

[25] O. C. Onar, J. Kobayashi, and A. Khaligh, "A fully directional universal power electronic interface for EV, HEV, and PHEV applications," *IEEE Trans. Power Electron.*, vol. 28, no. 12, pp. 5489–5498, Dec. 2013.

[26] T. K. Santhosh and C. Govindaraju, "Dual input dual output power converter with one-step-ahead control for hybrid electric vehicle applications," *IET Electr. Syst. Transp.*, vol. 7, no. 3, pp. 190–200, Sep. 2017.

[27] C. Duan, C. Wang, Z. Li, J. Chen, S. Wang, A. Snyder, and C. Jiang, "A solar power-assisted battery balancing system for electric vehicles," *IEEE Trans. Transport. Electrific.*, vol. 4, no. 2, pp. 432–443, Jun. 2018.

[28] F. Akar, Y. Tavlasoglu, and B. Vural, "An energy management strategy for a concept battery/ultracapacitor electric vehicle with improved battery life," *IEEE Trans. Transport. Electrific.*, vol. 3, no. 1, pp. 191–200, Mar. 2017.

[29] D. A. Savio, V. A. Juliet, B. Chokkalingam, S. Padmanaban, J. B. Holm-Nielsen, and F. Blaabjerg, "Photovoltaic integrated hybrid microgrid structured electric vehicle charging station and its energy management approach," *Energies*, vol. 12, no. 1, p. 168, Jan. 2019.

K. SURESH received the B.E. degree from Anna University, India, in 2010, and the M.Tech. degree in power electronics from Vel Tech University, in 2013. He is currently pursuing the Ph.D. degree from the SRM Institute of Science and Technology, India, with a focus on design of power electronic converters for electric vehicle applications. His research interests include design and control of power electronic converters, and renewable energy systems.

C. BHARATIRAJA (Senior Member, IEEE) was born in India, in 1980. He received the Master of Engineering degree in power electronics engineering from the Government College of Technology, Coimbatore, India, in 2006, and the Ph.D. degree in power electronics from the Faculty of Engineering, SRM Institute of Science and Technology, India, in 2015. He is currently an Associate Professor with the SRM Institute of Science and Technology, and pursuing a postdoctoral fellow research with the Department of Electrical and Computer Engineering, Northeastern University, USA. He has authored more than 50 articles which are published in international journal, including IEEE TRANSACTIONS. His research interests include multilevel inverters, new converter topologies, and control of power converters, SVPWM techniques for power converters and adjustable speed drives, electrical vehicle, wireless power transfer, and smart grid. He was an award recipient of prestigious Bhaskara Advanced Solar Energy (BASE), DST Government of India, and IUSSTF, Indo-U.S. Science and Technology Forum at 2017.

N. CHELLAMMAL (Member, IEEE) received the Master of Science degree in engineering in electrical drives and automation from Tashkent State Technical University, Russia, in 1996, and the Ph.D. degree in power electronics from the Faculty of Engineering, SRM institute of science and Technology, India. She is currently an Associate Professor with the SRM Institute of Science and Technology. Her main research interests include modeling of power electronic converters and drives, grid integration of renewable energy resources, and design of controllers.

MOHD TARIQ (Senior Member, IEEE) received the bachelor's degree in electrical engineering from Aligarh Muslim University, Aligarh, the master's degree in machine drives and power electronics from the Indian Institute of Technology (IIT)-Kharagpur, and the Ph.D. degree in electrical engineering with focus on power electronics and control from Nanyang Technological University (NTU), Singapore.

He is currently working as an Assistant Professor with Aligarh Muslim University, where he is directing various international and national sponsored research projects and leading a team of multiple researchers in the domain of power converters, energy storage devices, and their optimal control for electrified transportation and renewable energy application. Previously, he has worked as a Researcher at the Rolls-Royce-NTU Corporate Laboratory, Singapore, where he has worked on the design and development of power converters for more electric aircraft. Before joining his Ph.D., he has worked as a Scientist with the National Institute of Ocean Technology, Chennai, under the Ministry of Earth Sciences, Government of India, where he has worked on the design and development of BLDC motors for the underwater remotely operated vehicle application. He also served as an Assistant Professor at the Maulana Azad National Institute of Technology (MANIT), Bhopal, India. He has authored more than 130 research papers in international journals/conferences, including many articles in IEEE TRANSACTIONS/JOURNALS. He is also the Inventor of approximately 20 patents granted/published by the patent offices of USA, GB, India, and China.

He was a recipient of the 2019 Premium Award for Best Paper in *IET Electrical Systems in Transportation* Journal for his work on more electric aircraft and also the Best Paper Award from the IEEE Industry Applications Society's (IAS) and the Industrial Electronic Society (IES), Malaysia Section-Annual Symposium (ISCAIE-2016) held in Penang, Malaysia. He is a Young Scientist Scheme Awardee (2019) supported by the Department of Science and Technology, Government of India, and also a Young Engineer Awardee (2020) by the Institution of Engineers (India). He is also the Founder Chair of IEEE AMU SB and IEEE SIGHT AMU.

RIPON K. CHAKRABORTTY (Member, IEEE) received the B.Sc. and M.Sc. degrees in industrial and production engineering from the Bangladesh University of Engineering and Technology, in 2009 and 2013, respectively, and the Ph.D. degree in computer science from the University of New South Wales (UNSW) Canberra, Canberra, Australia, in 2017.

He is currently a Lecturer on system engineering and project management with the School of Engineering and Information Technology, UNSW Canberra. He has published a good number of journal articles and conference papers in well-reputed platforms. His research interests include wide range of topics in operations research, optimization problems, project management, supply chain management, and information systems management.

MICHAEL J. RYAN (Senior Member, IEEE) is currently a Professor and the Director of the Capability Systems Centre, University of New South Wales Canberra, Canberra. He lectures and regularly consults in a range of subjects, including communications systems, systems engineering, requirements engineering, and project management. He has authored or coauthored 12 books, three book chapters, and over 250 technical articles and reports.

He is a Fellow of Engineers Australia, the International Council on Systems Engineering, and the Institute of Managers and Leaders. He is the Co-Chair of the Requirements Working Group in the International Council on Systems Engineering (INCOSE).

BASEM ALAMRI (Member, IEEE) received the B.Sc. degree (Hons.) in electrical engineering from the King Fahd University of Petroleum and Minerals (KFUPM), in 2001, the M.Sc. degree in sustainable electrical power from Brunel University, London, U.K., in 2007, the M.Sc. degree (Hons.) in electrical power systems from King Abdulaziz University, Jeddah, Saudi Arabia, in 2008, and the Ph.D. degree in electrical power engineering from Brunel University, in 2017. He is currently an Assistant Professor of electrical engineering with the College of Engineering, Taif University. His research interests include power systems, power quality, power filter design, and smart grids, with a particular emphasis on the integration of renewable energy sources with power grids. He is a member of many international and local professional organizations. He is also a Certified Energy Auditor (CEA ®), a Certified Energy Manager (CEM ®), and a Certified Measurement and Verification Professional (CMVP ®) of the Association of Energy Engineers (AEE), USA. He has received many awards and prizes, including a certificate from the Advance Electronics Company (AEC) in recognition of the Outstanding Academic Achievement during the B.Sc. degree with KFUPM. He also received the National Grid (NG) Prize, the Power Grid Operator in the U.K., for being the top distinction student of the M.Sc. degree of the SEP Program with Brunel.